AIAA

AIAA 2005-4449

Towards Rocket Engine Components with Increased Strength and Robust Operating Characteristics

Bogdan Marcu
Ali Hadid
Pei Lin
Daniel Balcazar
The Boeing Company
Rocketdyne Propulsion and Power
6633 Canoga Avenue
Canoga Park, California

Man Mohan Rai
NASA
Ames Research Center
Moffett Field, California

Daniel J. Dorney .
NASA
Marshall Space Flight Center
Huntsville, Alabama

41st AIAA/ASME/SAE/ASEE Joint Propulsion Conference & Exhibit
10-13 July 2005
Tucson, Arizona

Towards Rocket Engine Components with Increased Strength and Robust Operating Characteristics

Bogdan Marcu, Ali Hadid, Pei Lin, Daniel Balcazar
The Boeing Company
Rocketdyne Propulsion and Power
6633 Canoga Avenue
Canoga Park, California

Man Mohan Rai
NASA
Ames Research Center
Moffett Field, California

Daniel J. Dorney
NASA
Marshall Space Flight Center
Huntsville, Alabama

Abstract

High-energy rotating machines, powering liquid propellant rocket engines, are subject to various sources of high and low cycle fatigue generated by unsteady flow phenomena. Given the tremendous need for reliability in a sustainable space exploration program, a fundamental change in the design methodology for engine components is required for both launch and space based systems. A design optimization system based on neural-networks has been applied and demonstrated in the redesign of the Space Shuttle Main Engine (SSME) Low Pressure Oxidizer Turbo Pump (LPOTP) turbine nozzle. One objective of the redesign effort was to increase airfoil thickness and thus increase its strength while at the same time detuning the vane natural frequency modes from the vortex shedding frequency. The second objective was to reduce the vortex shedding amplitude. The third objective was to maintain this low shedding amplitude even in the presence of large manufacturing tolerances. All of these objectives were achieved without generating any detrimental effects on the downstream flow through the turbine, and without introducing any penalty in performance. The airfoil redesign and preliminary assessment was performed in the Exploration Technology Directorate at NASA ARC. Boeing/Rocketdyne and NASA MSFC independently performed final CFD assessments of the design. Four different CFD codes were used in this process. They include WILDCAT/CORSAIR (NASA), FLUENT (commercial), TIDAL (Boeing Rocketdyne) and, a new family (Aardvark/Phantom) of CFD analysis codes developed at NASA MSFC employing LOX fluid properties and a Generalized Equation Set formulation. Extensive aerodynamic performance analysis and stress analysis carried out at Boeing Rocketdyne and NASA MSFC indicate that the redesign objectives have been fully met. The paper presents the results of the assessment analysis and discusses the future potential of robust optimal design for rocket engine components.

1. Introduction

One of the key requirements for sustainability of Space Exploration is the operational reliability and robustness of the systems deployed and used in space. In particular, the operation of propulsion systems based exclusively in space essentially requires systems which need minimal or no maintenance. This requirement forces the elimination of the current philosophy of operation for re-usable equipment, which is based on overhaul and repair at intervals in time dictated by the limits in the reliability of the system's components. In space there is limited or no access to repair or replace worn or damaged components. The absence of robust and reliable components will necessitate propulsion systems based on high redundancy with the associated cost and weight penalties.

These shortcomings can be avoided by a change in design paradigm for the components of space based propulsion systems. Here we propose a major role for formal multi-objective optimization methods in design optimization by embedding them in the standard design process. In order to obtain component designs that are simultaneously characterized by high performance, and high strength and robustness, the designer must cope simultaneously with a large number of design variables. The human mind can only simultaneously address a limited number of such variables in the context of a conventional design process. Formal optimization algorithms can handle a large number of design parameters and meet competing design requirements and objectives

The particular project described in the present report exemplifies how such an approach works and demonstrates the ability of the proposed design paradigm in providing a revolutionary increase in component strength, reliability, performance and robustness. Such improvements will be routinely required by future space based systems.

2. General description

High energy rotating machinery employed in liquid propellant rocket engines are subject to many sources of high cycle fatigue. Phenomena such as cavitation, manifold flow instabilities, stator-rotor interaction, and vortex shedding generate unsteady forces of various frequencies subjecting the hardware to high unsteady stress levels.

Particular attention has been focused on the phenomenon of vortex shedding at the trailing edge of turbine airfoils. Most published studies address cascade performance, with air or gas as a working fluid. Han and Cox [1] present, in quantitative detail, the shedding phenomenon on a turbine nozzle airfoil. They measure a range of Strouhal numbers at successively increasing cascade discharge velocities. More and Adhye [2] , Sieverding[3, 4] and Browand [5] showed that the shedding frequency and the size of the vortices are influenced by the nature of the boundary layer. These vortices have a significant effect on the shape and depth of the wake. Furthermore, the characteristics of vortex shedding have an impact on the interaction with the blade downstream. Contini et al [6] and Sieverding [4] suggest that the unsteady effects

associated with the trailing edge vortices are insufficiently understood and consequently not yet properly modeled. Sondak and Dorney [7, 8] showed that for a typical turbine cascade, the correct simulation of the flow separation at the trailing edge requires a grid of significant density (119 points at the trailing edge region). Also, in a stage configuration, the shedding frequency may either lock onto an upper harmonic of the blade passing fundamental frequency, or split into amplitudes at several harmonics.

While a large body of published literature addresses gas or air flow measurements, there is little available material regarding vortex shedding on cascades of airfoils/hydrofoils operating in liquid flows. Lee, Hah and Loellbach [9] performed a RANS CFD analysis of the unsteady flow interaction inside an axial flow pump stage. While blade load comparisons with experiments are presented, quantitative data pertaining to trailing edge vortex shedding is not included in this investigation. Busby et al [10] present numerical and experimental results for the same geometry with more details on the vortex shedding associated with the rotor blade row of the axial-flow pump. Their study shows rotor trailing edge shedding frequencies varying with radius (and blade thickness) and locking into the vane passing frequency harmonics. Ciocan et al [11] published detailed optical measurements (LDV and PIV) of the flow through a radial hydraulic turbine, however, without addressing the vortex shedding phenomenon.

The present report addresses the issue of a very energetic trailing edge vortex shedding phenomenon in an axial hydraulic turbine operating in liquid oxygen, namely the turbine powering the Low Pressure Oxidizer Turbo Pump (LPOTP) of the Space Shuttle Main Engine (SSME). The analysis presented here has been made in the very conservative context of addressing a flight safety issue for the Space Shuttle. In this study we present the CFD calculations carried out in support of a revolutionary redesign of the LPOTP turbine nozzle. Several CFD codes have been run simultaneously in order to determine and compare the frequency and amplitudes of shedding induced pressure fluctuations for the nominal and redesigned airfoils.

Insert 2 Man

Based on the CFD calculations, structural dynamics and stress calculations have been made in order to determine the expected safety factors and the expected life for the new component,and the impact on the entire turbopump..

Figure 1 shows a side view of the Space Shuttle Main Engine (SSME), and the location of the Low Pressure Oxidizer Turbo Pump (LPOTP).

Figure 2 shows a simplified schematic of the engine. A cross section of the LPOTP is shown in Fig. 3. The pump side of the LPOTP consists of a single piece inducer powered by a six stage hydraulic turbine. The turbine is fed via a tap-off line from the discharge of the High Pressure Oxidizer Turbo Pump (HPOTP). The discharge of the LPOTP turbine is re-circulated back to the inlet of the HPOTP.

Figure 4 shows the exact location of the LPOTP turbine nozzle. Metallurgical inspections of the nozzle parts have found evidence of high cycle fatigue (HCF) at the nozzle trailing edge near the end walls. Analysis of the known sources of excitation of HCF points to vortex shedding as the most probable cause. Strong vortex shedding can generate flapping of the trailing edge as shown in the detail in Fig.4. Indeed, CFD analyses which will be presented in the next sections show that shedding frequencies are close to the the blade trailing edge flapping mode natural frequency..

The LPOTP turbine nozzle component is currently being replaced at carefully monitored time intervals ensuring full safety for the Shuttle flights. If the same turbopump were to operate within a space based system, the HCF wear of the part would limit the operational life of the overall system. Clearly, it is imperative that reliability and robustness are built into the components for space based propulsion systems.

3. CFD Analysis

The flow analyses presented in this study have been performed using several CFD codes.The NASA MSFC Corsair family of codes were used during the initial phase of the project These codes solve the time-dependent, three-dimensional Reynolds-averaged Navier-Stokes equations. The numerical algorithm used in the computational procedure consists of a time-marching, implicit, finite-difference scheme. The procedure is spacially third-order accurate and temporally second-order accurate. The inviscid fluxes are discretized according to the scheme developed by Roe [12]. The viscous fluxes are calculated using standard central differences. An approximate-factorization technique is used to reduce and simplify the matrices which need to be solved at every time step. Newton sub-iterations are used at each time step to enhance stability and reduce linearization errors. The equations of motion are extended to turbulent flows using an eddy viscosity formulation. The turbulent viscosity is calculated using the two-layer Baldwin-Lomax algebraic turbulence model [13]. The computational procedure uses O- and H-type zonal grids to discretize the flow field and facilitate relative motion between rotor and stator rows. The O-grids are body-fitted to the surfaces of the airfoils and generated using an elliptic grid generator. They are used to accurately resolve the viscous flow in the blade passages and to easily apply the algebraic turbulence model. The algebraically-generated H-grids are used to discretize the remainder of the flow field. Details of the algorithms and the gridding methodology can be found in references [14, 15 and 16].

Calls to Message Passing Interface (MPI) and OpenMP parallel computation libraries have been implemented in the code to reduce the computation time for large-scale three-dimensional simulations. The use of MPI allows the coupling of different geometric components, such as a turbine cavity, in a straightforward manner.

The Corsair family of codes has been exhaustively validated for gas turbine analysis. In the present study however, the codes have been used to analyze a turbine geometry operating in liquid. While the input parameters have been carefully crafted to best approximate the actual flow conditions, the speed of sound in the working fluid could not be accurately scaled. Due to this limitation, analyses of the LPOTP turbine have initially been limited to the first turbine stage; further expansion of the computational domain to include more stages downstream would have led to density effects that would result in a departure of the computed solution from the actual physics.

With the above limitations in mind, a newer code has been used for the present analysis. The NASA MSFC Aardvark code employs a compressible/incompressible formulation based on the Generalized Equation Set [17, 18] formulation for the Reynolds Averaged Navier Stokes equations. A preconditioning algorithm is used for incompressible flows. The new algorithm utilizes the true thermodynamic properties of the working

fluid. A library of real fluid properties has been implemented into the code.

The results obtained with Corsair and Aardvark are very similar, displaying the same trends and changes in pressure fluctuation frequencies and amplitude. However there are small quantitative differences in surface pressures, shedding frequencies and amplitudes. The two codes are to some extent numerically related to each other (the airfoil topology is modeled with the same type of grids, while the zonal boundary condition implementation follows similar logic, and the same turbulence model is used). Hence two additional codes utilizing different turbulence models and based on unstructured grids have also been used for analysis.

The Tidal code, which stands for Time Iterative Density/pressure based Algorithm, is a RANS code developed at Rocketdyne. The code utilizes a finite volume, multi-zone method, and a steady/unsteady modularized flow simulation algorithm. A unified approach is employed to combine the density- and pressure-based methods to enable the computation of flow fields ranging from incompressible to supersonic flows. In the present analysis, a dual time-stepping method is used to obtain a time-accurate solution. A central difference scheme is applied to the convection terms and viscous term. An adaptive second order dissipation method is employed for smoothing. The 2-equation k-ε turbulence model is used. Precondition is used in the analysis. Parallel processing on a Linux cluster enables a rapid turn-around.

The commercial code FLUENT has also been used here for 2D single airfoil and 2D full stage analysis. FLUENT is a general purpose computer program for modeling fluid flow and heat transfer in complex geometries. It provides complete mesh flexibility in solving flow problems with unstructured meshes in 2D and 3D geometries using triangular/tetrahedral, quadrilateral/hexagonal, or mixed (hybrid) grids that includes prisms and pyramids. The mesh can be generated about complex geometries with relative ease using the preprocessor package GAMBIT. FLUENT allows for multiple moving reference frames, including sliding mesh interfaces and mixing planes for the modeling of rotor/stator interaction. The segregated solver formulation was used to solve the continuity, momentum and scalar equations sequentially. Second order spatial accuracy and implicit second-order time stepping were used to reduce spatial and temporal discretization errors.

A refined unstructured mesh near the blade surface and downstream of the trailing edge together with a small time step size were used in order to accurately capture the shedding frequency and amplitude of the LPOTP turbine nozzle. Great care was exercised to ensure grid and time-step independent solution by refining the grid and choosing a small time step of the order of 1/50 of a shedding period. The number of sub-iterations per time step was chosen large enough to ensure convergence at each time step.

Turbulence effects were captured using the unsteady Reynolds Averaged Navier-Stokes (URANS) full Reynolds stress model (RSM) of Launder, Reece and Rodi [19]. In this model the full transport equations for the turbulent Reynolds stresses are solved together with the continuity and momentum equations. The sliding mesh capability of FLUENT is used to predict the time dependent flow through a 2D rotor-stator blade row. The time-varying rotor-stator interaction is modeled by allowing the mesh associated with the moving rotor to translate (slide) relative to the stationary mesh associated with the stator blade. Initially a steady flow calculation with a stationary rotor was initiated and the solution obtained was used as a starting solution for the time dependent sliding-mesh calculation. Unsteady lift forces on the rotor and the stator blades were monitored to determine when the unsteady flow predictions became time-periodic and independent of the initial condition.

4. Nominal Geometry Analysis. HCF induced by vortex shedding

Figure 5 shows the flow field through the LPOTP nozzle cascade obtained using Wildcat. Entropy is used to visualize the vortex shedding patterns at the airfoil's trailing edge. The result was obtained from a simulation of the flow through a 43 airfoil cascade, at a pressure drop corresponding to 109% Rated Power Level (RPL) of the SSME. Unlike cylinder vortex shedding, the shedding at the trailing edge of the nozzle creates alternating vortices of unequal strength: the vortex released from the pressure side of the vane is stronger. The effect of the pressure unsteadiness is felt upstream of the trailing edges, as seen on the vane pressure loading envelopes in Fig. 6. Significant unsteadiness at the trailing edge region can be deduced from the large excursions in the pressure envelope. The effect is felt on the suction side for almost two thirds of the blade chord from the trailing edge. The frequency and amplitude of the

vortex shedding are shown on the FFT diagram in Fig. 7. Fifty points out of the 301 grid points around the blade were sampled, and the location with the maximum amplitude of pressure fluctuation was selected (the point is located at the tangency point where the trailing edge circle meets the pressure side of the airfoil). The results indicate a point pressure fluctuation of ±181 psi at a frequency of 44,175 Hz. This large amplitude diminishes rapidly as one moves away from the point of maximum amplitude (the corresponding tangency point on the suction surface has a slightly lower amplitude at the same frequency). Hence a more meaningful measure of unsteady stress is the frequency and amplitude of fluctuating pressure averaged over a 0.100 inch width section along the airfoil's trailing edge. This averaged measure has an amplitude of ± 57 psi at the same frequency of 44,174 Hz.

Figure 8 shows the flow field obtained from a 2-D CFD Wildcat simulation of a stage configuration. The first stage of the LPOTP turbine is modeled with 44 nozzles and 66 blades (2-nozzles and 3-blades) operating at 109% RPL of the SSME. The vortex patterns due to shedding are clearly visible in the wakes all the way through the rotor row inlet. There, the vortices interact with the rotor blade, impinging on the leading edges, and then being convected downstream through the rotor passage. The spectral content of the pressure fluctuation at the tangency point on the pressure side of the nozzle is shown in Figure. 9. The results obtained from the Wildcat and Aardvark simulations are compared in this figure. The data show fluctuating pressure amplitudes of ±212 psi at a frequency of 45487 Hz from Wildcat and ±208 psi at 43592 Hz from Aardvark. The frequency and amplitude values are very close for the two codes.

A comparison of the results obtained using Wildcat for the cascade and stage configurations (Figure 7 and 9) show differences in shedding characteristics. The shedding frequency for the stage configuration is slightly different than the shedding frequency for a vane in isolation because of a lock-in effect. The shedding frequency locks on to the closest upper harmonic of the vane passing fundamental frequency, or to the closest upper harmonic and a half [10]. In this case the Wildcat simulation indicates a lock into the 12th harmonic, while the Aardvark simulation indicates a lock into the 11th + ½. It should be noted that the results obtained

with the two different codes are very close. The Strouhal number based on local velocity at the trailing edge and the trailing edge thickness is St = 0.223-0.235. The pressure amplitude averaged over the 0.100 inch section at the trailing edge is ±72 psi (Aardvark simulation).

Figure 10 shows the nozzle vane response as a function of frequency for the trailing edge flap mode, and the spectral content of the vortex shedding phenomenon at 109% engine Rated Power Level (RPL). The vane peak resonance response value displayed corresponds to the natural frequency of the nominal geometry as measured in the lab at 47 kHz without corrections for LOX mass flow effects which can account for 20%-40% reduction in frequency [21]. Additional uncertainty comes from the actual hardware which has large deviations from the nominal airfoil geometry. Overall, with all the corrections and variations due to hardware geometry deviations, the blade natural frequency associated with the trailing edge flap mode can range anywhere between 24 kHz and 46 kHz. The vortex shedding frequency (43.6 kHz) in Figure 10 represents the value obtained with Aardvark for the nominal geometry. Several CFD calculations have been performed for nozzles with variations in geometry representative of hardware variations in vane trailing edge thicknesses. Furthermore, CFD calculations for cylinders have been performed [20] at similar Reynolds numbers (based on local TE velocity and TE diameter) in order to calibrate the code output for fluctuation frequencies. The results indicate an over-prediction of shedding frequency by 15-20%. These uncertainties in the computed data and the hardware geometry result in a shedding frequency range between 28 kHz and 45 kHz. Thus the shedding frequency range and the vane natural frequency range overlap. This overlap and the lock-in mechanisms observed many times in operation [7, 8, 10] are a strong indication that vortex shedding is the major cause for HCF wear and damage observed in the operation of the LPOTP.

5. The traditional redesign approach and its shortcomings

The initial approach taken to address the resonance problem consisted of a "retrofit" of the existing shelf parts. The details are discussed at length in reference [21]. At the expense of a small percentage of the overall turbine performance, a shortening of the LPOTP nozzle airfoil via machining was considered for the purpose of

decoupling the vortex shedding from the flap mode of the vane TE. Shortening of the blade, results in a thicker trailing edge, and consequently, the vortex shedding frequency decreases, while the stiffness and hence the trailing edge flap natural frequency increase.

In the following we will briefly present the shortcomings of this retrofit approach.

After several trade-off analyses, a vane cut of 0.100 inch in length at the trailing edge was found to provide a sufficient increase in trailing edge thickness. Figure 11 shows the baseline and retrofit first stage turbine geometries. The cut cannot be accomplished uniformly over the entire vane span because the cutting tool has no access near the end walls. Consequently there is a round cut towards the walls.

Figure 12 shows a snapshot of the flow field through the turbine stage for both the baseline and retrofit geometries at midspan. The thicker trailing edge of the retrofit nozzle and the sharp edges left after the cut (only limited chamfer can be achieved) produce a lower vortex shedding frequency (evidenced by the lower density of blobs convected downstream) but stronger vortices (evidenced by the sharper color contrast in the plot ###).

Figure 13 displays the quantitative effects of the modification. On the one hand, the objective of reducing the shedding frequency is achieved for the nozzle vane, as shown in Figure 13a: the shedding frequency has been lowered by about 17 kHz, from 44 kHz to 28 kHz. Modal analysis and lab tests for the modified nozzle vane indicate trailing edge flap mode natural frequencies as high as 65-70 kHz, which reduces to about 52 kHz in operation after accounting for the LOX mass flow effect. Thus a frequency separation of 24 kHz is achieved.

Paragraph required. (couple to ###)

Unfortunately, Figure 13b shows that the nozzle problem has been solved at the expense of the rotor blade downstream. Stronger vortices shed by the cut back vane at lower frequency are convected into the rotor passage. These vortices impinge on the rotor with enough energy to create a strong disturbance at a frequency of 29 kHz. The frequency of this disturbance lies in the middle of the frequency range for the rotor blade first bending mode natural frequency. This is not acceptable. Therefore, the retrofit solution has been rejected.

It is expected that the redesign of the baseline airfoil using traditional design techniques will yield a new and thicker airfoil that has a lower shedding frequency but a larger shedding amplitude. This amplitude may not be as large as that produced by the cutback vane, but large enough to surface as a disturbance amplitude at an undesired frequency on the rotor blade downstream.

I3 insert Man

6. New, extended design requirements

The design requirements for a new nozzle airfoil should therefore contain additional provisions for preventing or limiting the introduction of unintended downstream perturbations. Obviously the overall turbine performance must be preserved in order to ensure the proper operation of the turbopump component.The complete set of design requirements can be summarized as follows:

- The airfoil should be as thick as possible at the TE, thereby increasing the natural flap mode frequency, and decreasing the shedding frequency, thus decoupling the two frequencies in operation

- Steady state (time averaged) flow conditions at nozzle row discharge should be preserved:

  - same nozzle throat area in order to conserve LOX mass flow value.

  - same discharge flow angle in order to conserve downstream-rotor blade work.

- Additional flow disturbances should not be introduced downstream:

  - control of flow separation at the nozzle TE

  - diminished the shedding amplitude

- Airfoil shedding should be insensitive to geometry discrepancies due to manufacturing or wear and tear

  - Expected manufacturing method: casting with ± 0.006 inch tolerance with large variations

The last requirement has been added as a result of large variations in the current hardware geometry with the intention of partially removing the operational performance sensitivity to airfoil geometry deviations.

This set of requirements is extremely complex, and difficult, if not impossible to achieve within the context of traditional design techniques. Thus, it

constitutes an excellent case for formal design optimization methodology. Drawing on previous results from collaborations between NASA ARC Exploration Technology Directorate and Rocketdyne, the SSME LPOTP Nozzle redesign team decided to address the redesign task by utilizing design optimization technology developed at NASA ARC. The airfoil redesign and preliminary assessment was performed in the Exploration Technology Directorate at NASA ARC. Boeing/Rocketdyne and NASA MSFC independently performed final CFD assessments of the design

7. **Optimization methodology. The new airfoil geometry**

[Man, insert 4 + figs]...

Figure 14 shows the new design overlaid on the baseline nozzle design for comparison. This geometry is the result of five design iterations and is referred to as O5 in the rest of the text. The airfoil is very thick, and in particular, the trailing edge thickness is increased by about 60% Intuitively one would expect such an increase in thickness to introduce a significant change in the wake profile and consequently a change in the flow downstream of the nozzle row. A significant amount of analysis, presented in the following sections, was performed to determine if the new airfoil produced any detrimental changes in the flow downstream.

8. **CFD Analysis of performance**

8.1 **Nozzle Performance**

Figure 15 presents a comparison of the nozzle vane pressure loading, for the baseline and optimized airfoils. One observes that while the baseline airfoil loading occurs mostly on the last two thirds of the axial chord, the optimized airfoil distributes the load more uniformly. A vertical line marks the proximity of the trailing edge in both plots. A significant difference exist in the pressure difference between the pressure side and the suction side at the marked location; a larger Δp for the baseline geometry and a diminished Δp for O5.

Figure 16 is a carpet plot comparing the level of unsteadiness in pressure oscillations at different locations on the airfoils. The plot should be interpreted as follows: the x axis represents frequency, in Hz, the y axis represents locations

around the airfoil, starting and ending at the leading edge, and the z axis represents the amplitude of the pressure fluctuation at each point. The plot shows a reduction in shedding frequency from 43.1 kHz to 32.7 kHz, and a remarkable reduction in the overall amount of unsteadiness for the O5 profile. The new reduction provides a reduction of 76% in peak amplitudes near the trailing edge.

The data in figures 15 and 16 were obtained from Aardvark

Figure 17 shows a similar comparison but obtained from a 3-D Tidal simulation at midspan. In this computation pressure fluctuations were recorded at a location near the vane trailing edge, where Aardvark and Wildcat showed maximum amplitudes for the baseline and O5 airfoils. The plot shows the fluctuations for O5 are about 50% less than the fluctuations for the baseline, with a corresponding frequency decrease from 35 kHz to 25 kHz.

Figure 18 shows results obtained from 2-D FLUENT computations, where data has been sampled as in the Tidal computation, i.e. at a location near the vane trailing edge, where Aardvark and Wildcat showed maximum amplitudes for the baseline and O5 airfoils. This plot shows a 52% reduction in amplitude for the O5 vane with a corresponding reduction in frequency from 56 kHz to 47 kHz. FLUENT yields shedding frequencies which are clearly higher than physical, given the calibration runs made for cylinders using Aardvark (no calibration runs were made for cylinders using TIDAL or FLUENT).

The important feature in figures 16 through 18 is a consistent trend obtained with a variety of CFD codes. The O5 vane reduces pressure fluctuation amplitudes by 50-75% while reducing the shedding frequency by about 10 kHz.

8.2 **Overall Turbine Performance**

Figures 19 and 20 compare the 1st stage rotor blade loading and 2nd stage stator loading at 109% engine RPL. Each plot overlays the pressure loading for the configurations using the baseline and the O5 nozzles. Both plots indicate insignificant changes in rotor blade and stator vane loadings downstream. It is reasonable to assume that if only small changes can be observed in the two downstream rows following the replaced nozzle, even smaller changes in performance are to be expected further downstream and therefore

the nozzle replacement produces little or no change in turbine performance

8.3 Downstream Unsteady Flow Analysis

Figure 21 shows a comparison of the unsteady tangential force on the 1st stage rotor blade obtained from Aardvark. The FFT analysis for the time varying tangential force is shown in this figure. The fundamental frequency for the stage configuration is the vane passing frequency of 3.79 kHz corresponding to 44 nozzle vanes in the simulation. The use of O5 instead of baseline nozzle airfoil decreases the amplitude at this frequency from ±8.8% of the mean value to ±6.8%. Additionally, O5 *does not* introduce additional disturbances other than the small amplitude disturbances similar to those observed for the baseline design. This is a significant accomplishment given that the TE thickness of O5 is significantly larger that that of the baseline airfoil.

Given the importance of limiting or perhaps even reducing the disturbances introduced downstream compared to the baseline case, the Tidal and FLUENT codes were also used in this analysis. The results of these analyses are given below:

Figure 22 shows the FFT analysis of the unsteady tangential force on the rotor blade obtained from Wildcat. The plot indicates a reduction in amplitude from ±19% to ±12% at fundamental frequency and diminished amplitudes at higher frequencies with the use of O5.

Figure 23 shows the same analysis using data produced by TIDAL. The amplitude at the fundamental frequency is practically unchanged in this calculation (a slight reduction from ±4.2% to ±3.8%) while the high frequency amplitudes remain very small (less than 0.5% of average) with the use of O5.

In Figure 24, the analysis is repeated for data produced FLUENT. FLUENT shows no change in the amplitude at the fundamental frequency (±19.5%) and no additional disturbances introduced at higher frequencies with the use of O5.

The simulation results provided by codes with different numerical schemes, different grid structures and different turbulence models all display a consistent trend: *there is a modest benefit or no change downstream of the nozzle row when the current baseline nozzle geometry is replaced by the O5 airfoil*. These results have built confidence in the capabilities of the new design.

8.4 Robustness in operation

(Man insert 5)

9. Structural dynamics analysis.

An exhaustive amount of analysis for assessing the structural dynamics of the new design has been performed. Only the most important aspects are included in this paper.

Figure 25 shows the TE flap mode response, corrected for a 30% LOX mass flow effect, for both the baseline and the O5 airfoils. The frequency ranges associated with the vortex shedding at 109% engine RPL for the baseline and O5 airfoils are also shown in the figure. Flow data was obtained from Aardvark for airfoils at the extremes of hardware geometry variation and adjusted by a 20% frequency shift based on calibration using cylinder simulations. The O5 performance is treated in a conservative manner, in the sense that although this geometry is characterized by exceptional robustness, and minimum variation in flow performance due to geometry variation, the same percent statistical bounds are applied on vortex shedding frequencies as for the baseline configuration. The plot clearly shows the good separation in shedding and flap mode natural frequencies for the O5 geometry at 109% engine RPL regime. A comparison of figures 10 and 25 shows the significant increase in frequency separation with the use of O5.

Figure 26 is an elaboration of the information in Figure 25 throughout the throttling range of the SSME engine. The plot shows the range of frequencies associated with the baseline geometry in blue fields and the ones associated with the O5 geometry in purple. CFD simulations have been performed for the flow regimes corresponding to 64.5%, 80%, 104% and 109% engine RPL, with intermediate RPL point performance obtained via a cubic spline fit. The data processed for the chart contains all the corrections for the uncertainties related to the flow conditions, LOX mass flow effects and possible alterations in the manufactured geometry of the hardware, and thus the large range of frequency values for both geometries. Again, the data is processed taking the conservative approach typical for analysis of man-rated propulsion hardware such as SSME. One can observe that

the baseline design geometry shedding frequency ranges interfere significantly with the natural vane frequency associated with the TE flap mode at all engine RPL regimes. In spite of the conservative estimate of the performance for O5, a large margin of 27% is obtained as separation between frequencies at the highest RPL regime considered (109%). With this margin, the frequencies are considered completely detuned.

10. Stress analysis.

Similar to the structural dynamics section, only some principal results are presented here from the large amount of stress analysis done for this project. Besides pressure loads induced by the steady state and unsteady aerodynamic phenomena, additional loads generated by the engine vibration, static loads transmitted through the turbopump support structure and mechanical and thermal loads during transients have been included in the analysis.

Table 1 summarizes some of the main results for the nozzle vane, showing the overall change in stress resulting from the replacement of the baseline geometry with the O5 geometry. The various categories of stress considered are reduced by 19% to 600% generating an overall increase in the safety factor from 3.5 to 6.3 and thus giving the part fitted with the O5 airfoil an essentially infinite life in operation.

Figure 27 shows the locations of peak cumulative stress (steady state + alternate) on the rotor blade. The locations are near the leading edge (Figure 27 a) and trailing edge (Figure 27 b). The maximum occurs in the leading edge region where the calculated factor of safety is 4.91 for the baseline design configuration and 6.31 for the O5 configuration, an increase by 28% in safety.

These results constitute an essential element of support for the design methodology for components of space based propulsion systems. Without any penalty in performance, a component designed via multi-objective optimization methodology has resulted in almost a 100% increase in strength, robust operation and practically infinite life.

11. Contribution potential for Space Exlploration Missions

The methodology presented here can be applied to airfoil design for all turbomachinery equipment developed for space operations. Based on detailed analysis identifying all sources of intense stress, LCF and HCF, including provisions necessary for deep throttling of rocket engines, design requirements similar to the extended design requirements presented in section 6 can be formulated. Subsequent airfoil design using optimization methodology as presented here will ensure increased strength and robust operating characteristics for the components designed.

Given the powerful algorithms which form the foundation of the optimization methodology demonstrated here, one can extend its application to other components of space based systems and subsystems. Principal candidates are those components deemed the most fragile in operation, for example, seals of various kinds, bearings, injectors, or valves.

The same methodology can be applied on a larger scale, and earlier in the evolution of a mission conceptual design, for trade-off studies. Mission formulation, vehicle/platform architecture and space flight procedures can be parameterized using large sets of variables modeling all necessary aspects. Multi-objective optimization can be performed in high-dimensional design spaces that include all the necessary variables. *"Optimize-not-compromise" should become the motto of conceptual thinking for all future space exploration architectures.*

12. Conclusions.

A design methodology based on formal multi-objective optimization technology has been applied and demonstrated for the redesign of the SSME LPOTP turbine nozzle. The new nozzle design has achieved about 100% increase in strength, significantly extended life in operation and an elevated robustness in operation while the overall turbine performance has been maintained the same as for original design.

The design methodology is proposed as a standard design procedure for components of space based systems as it provides a means to design such components with significantly improved strength, reliability and robust operating characteristics.

13. References

1 Han, L. S. and Cox, W. R., "A visual Study of Turbine Blade Pressure-Side Boundary Layers",

ASME Journal of Engineering for Power, Vol. 105, 1983, pp. 47-52.

2 Moore, J. and Adhye, R., "Secondary flows and losses downstream of a turbine cascade", *Journal of Engineering for Gas Turbines and Power*, Vol. 109, 1985, pp. 961-969.

3 Sieverding, C. H., "Recent progress in understanding of basics aspect of secondary flows in turbine blade passages", *ASME, Journal of Eengineering for Turbines and Power*, Vol. 107, 1985, 248-257.

4 Sieverding, C. H., and Heinemann, H., "The influence of boundary layer state on vortex shedding from flat plates and turbine cascades", *ASME paper 89-GT-296*, 1989.

5 Browand, F. K., "Factors affecting vortex shedding on airfoils", Private communication, 2002.

6 Contini, D., Manfrida, G., Michelassi, V. and Riccio, G., "Measurements of Vortex Shedding and Wake Decay Downstream of a Turbine Inlet Guide Vane", *Flow Turbulence and Combustion*, Vol. 64, 2000, pp. 235-278.

7 Sondak, D. L., and Dorney, D. J., ``Vortex Shedding in a Turbine Cascade," *International Journal of Turbo and Jet Engines,* Vol. 16, No. 2, 1999, pp. 107-126.

8 Sondak, D. L., and Dorney, D. J., ``Simulation of Vortex Shedding in a Turbine Stage," *ASME Journal of Turbomachinery*, Vol. 121, July, 1999, pp. 428-435.

9 Lee, Y-T., Hah, C. and Loellbach, J., "Unsteady Flow Interaction Inside a High-Reynolds-Number Axial-Flow Pump Stage", AIAA Paper 98-0970, 1997.

10 Busby, J. A., Taylor, L. K., Jiang, M. and Whitfield, D. L., "Unsteady 3-D Incompressible Flow Interaction in Multiple Blade-Row Turbomachinery", *AIAA Paper 98-0423*, 1998.

11 Ciocan, G. D., Avellan, F. and Kueny, J-L., "Optical Measurement Techniques for Experimental Analysis of Hydraulic Turbine Rotor-Stator Interaction", Proceedings of the ASME 2000 Fluids Engineering Division

Summer Meeting, June 11-15, 2000, Boston, Massachussetts.

12 Roe, P. L., ``Approximate Riemann Solvers, Parameter Vectors, and Difference Schemes," *Journal of Computational Physics*, Vol. 43, 1981, pp. 357-372.

13 Baldwin, B. S., and Lomax, H., ``Thin Layer Approximation and Algebraic Model for Separated Turbulent Flow," AIAA Paper 78-257, Huntsville, AL, January, 1978.

14 Rai, M. M., "Navier-Stokes Simulations of Rotor-Stator Interaction Using Patched and Overlaid Grids," AIAA Journal of Propulsion and Power, Vol.3, No.5, pp.387-396, 1987.

15 Rai, M. M., "Three-Dimensional Navier-Stokes Simulations of Turbine Rotor-Stator Interaction; Part I - Methodology," AIAA Journal of Propulsion, Vol. 5, No. 3, 1989, pp. 305-311.

16 D.J.Dorney and R.L. Davis, "Numerical Simulations of Unsteady Transonic Flows in Turbomachines", AIAA paper 94-2833.

17 C. L. Merkle, V. Sankaran, D. J. Dorney, and D. L. Sondak, "A Generalized Fluid Formulation for Turbomachinery Computations", AIAA Paper 2003-3999

18 Sondak, D. L., and Dorney, D. J., "General Equation Set Solver for Compressible and Incompressible Turbomachinery Flows", AIAA paper 2003-4420

19 Launder B. E., Reece G. I. and Rodi W., 'Progress in the development of a Reynolds stress closure', J. Fluid Mech., vol. 68, 1975

20 Peugeot, J.W. and Dorney, J. D., "Investigation of Vortex Shedding behind a Cylinder Using Wildcat and Aardvark CFD Codes.", Private Communication, 2003.

21 Marcu, B., Balcazar, D., Zdenek, C.D., Lunde, K. J., Dorney, D. J., "Vane Vortex Shedding Effects on SSME LPOTP Turbine", Proceedings of the 52nd JANNAF Interagency Propulsion Committee Meeting, Las Vegas, NV, 10-13 May, 2004
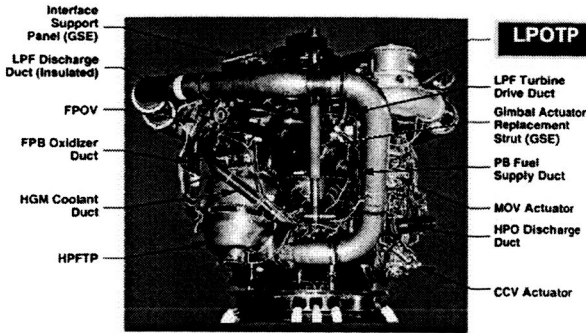
Figure 1: Side view of the Space Shuttle Main Engine (SSME), with the location of the Low Pressure Oxidizer Turbopump (LPOTP)
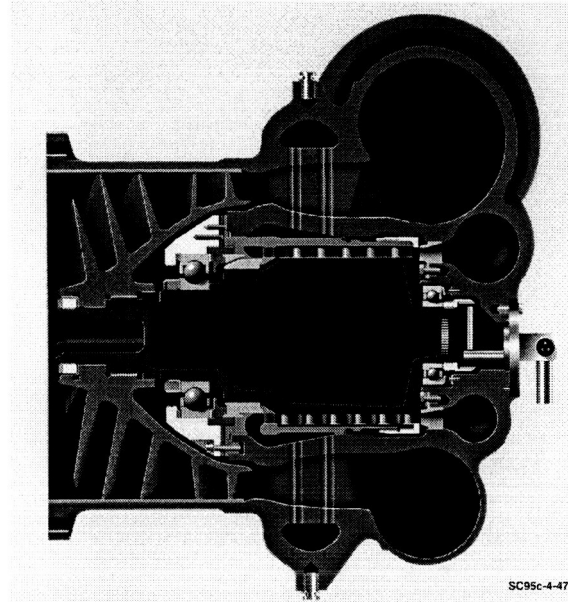

Figure 2. SSME Schematic.

Figure 3. Cross-section of the LPOTP. The turbine is fed by tapping high pressure liquid oxygen from the main oxidizer pump discharge and routing it into the turbine inlet via channels drilled through the mounts. Feed pressure during operation is around 4000 psi.
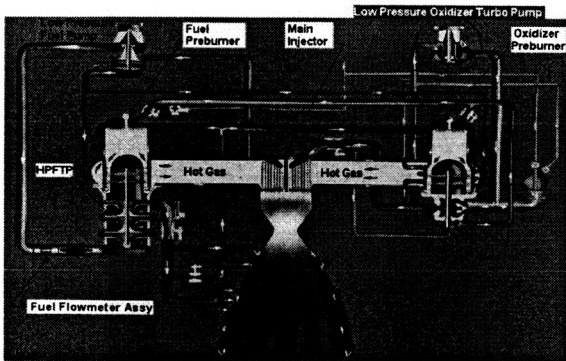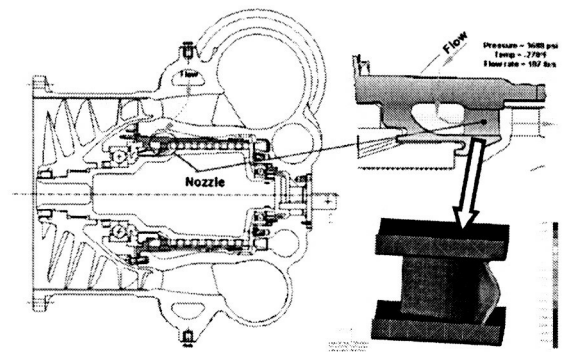

Figure 4. Schematic of the SSME LPOTP with the location of the turbine nozzle. Insert shows the airfoil trailing edge flapping mode.

Figure 7 FFT analysis of the pressure fluctuation at the point of maximum fluctuation amplitude. Wildcat cascade analysis.

Figure 5: Vortex shedding on the SSME LPOTP turbine nozzle, baseline nominal geometry. Shown is the entropy field. Wildcat cascade analysis.

Figure 8. Vortex shedding on the SSME LPOTP turbine nozzle, baseline nominal geometry, stage configuration. Shown is the entropy field. Wildcat stage unsteady analysis.

Figure 6: Nozzle pressure loading: time averaged, minimum and maximum pressure envelope. Wildcat cascade analysis.
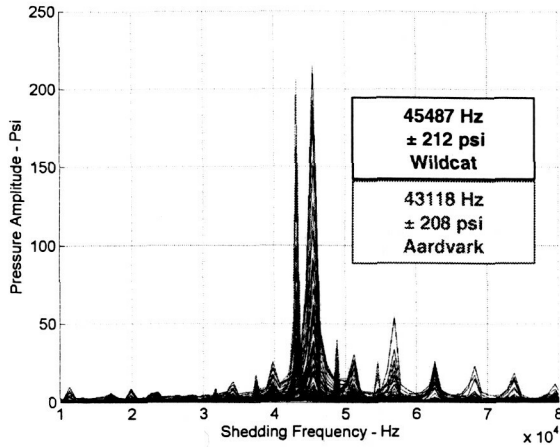
Figure 9. FFT analysis of the pressure fluctuation at the point of maximum fluctuation amplitude on the nozzle in the stage configuration. Wildcat vs. Aardvark solution comparison.

Baseline geometry
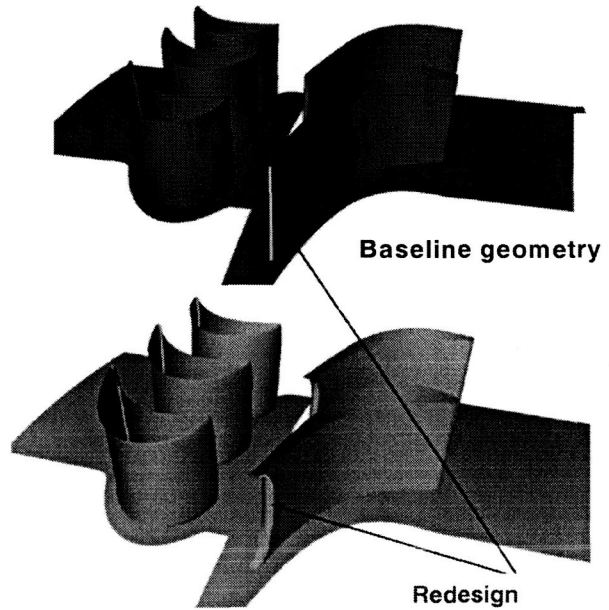
Redesign

Figure 11. Nozzle retrofit design: 0.100 cut-back at vane trailing edge. The round shape of the cut is dictated by lack of access for the cutting tool near the end-walls. A portion of first turbine stage is shown here in a model.
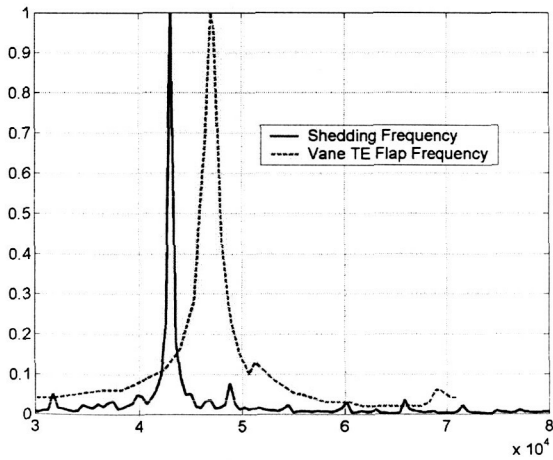
Figure 10. Vane vortex shedding versus vane trailing edge flap mode natural frequency. The TE flap mode frequency value shown (47 kHz) was measured in air, no correction is applied for lox mass flow effect (which would reduce the frequency by 20%-40%). Vortex shedding frequency shown is Aardvark 2-D CFD solution, without correction (cylinder vortex shedding runs indicate 15%-20% over-prediction).
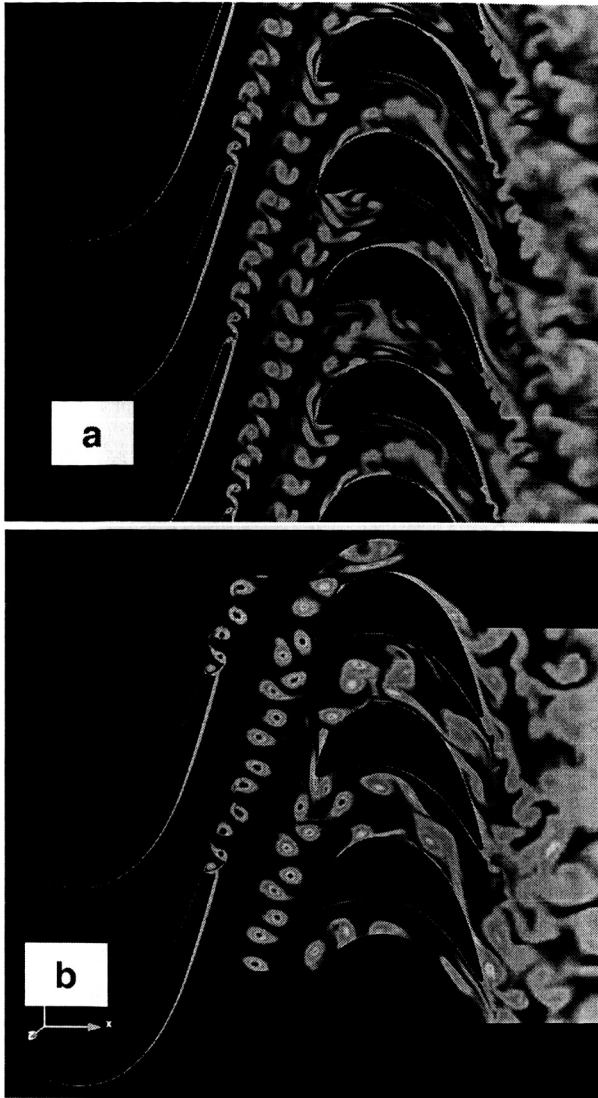
Figure 12. Comparison between the flow through the baseline first stage turbine geometry (a) and the retrofit modified geometry (b). Shown is 2-D Aardvark CFD solution.
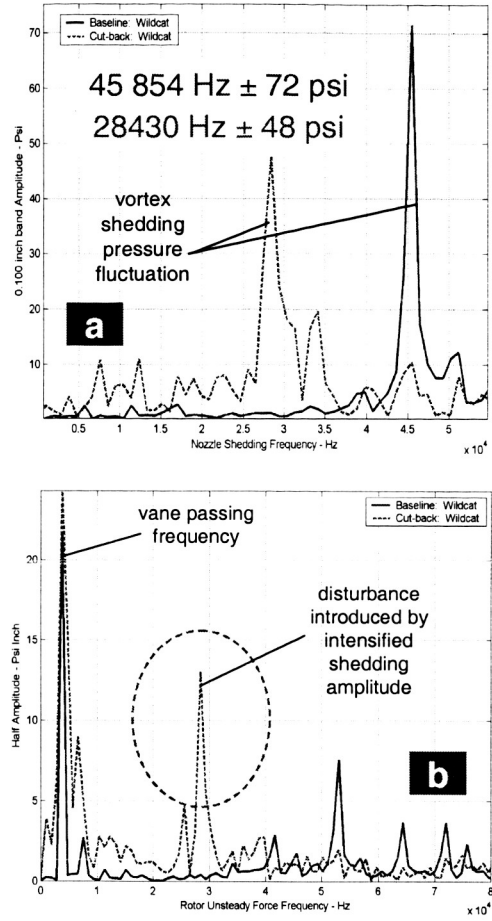
Figure 13. Vane cut-back effects: a) Shedding frequency is reduced by 14 kHz on a 0.100 band at the trailing edge of the vane but b) a new and strong disturbance is introduced downstream evidenced by the large amplitude at 29 kHz on the blade tangential force spectral analysis. 2-D Aardvark CFD solution.
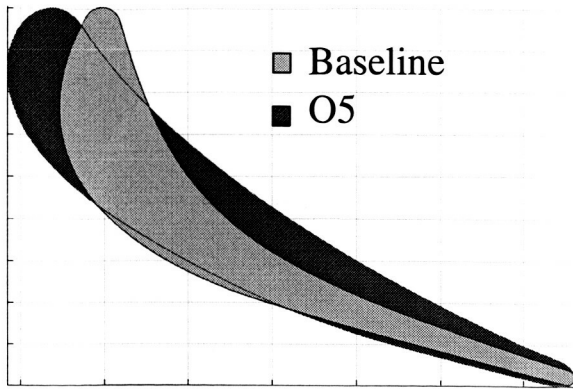
Figure 14. Vane redesign via optimization: over-plot of baseline geometry versus optimized geometry. Trailing edge thickness is increased by almost 100%.

Figure 16. Comparison of unsteady pressure fluctuation during operation on the nozzle vane. Data has been sampled at 50 points around the vane from Aardvark 2-D CFD solution. O5 vane displays significantly reduced unsteadiness.

Figure 15. Vane pressure loading at 109% engine RPL a) baseline geometry b) O5
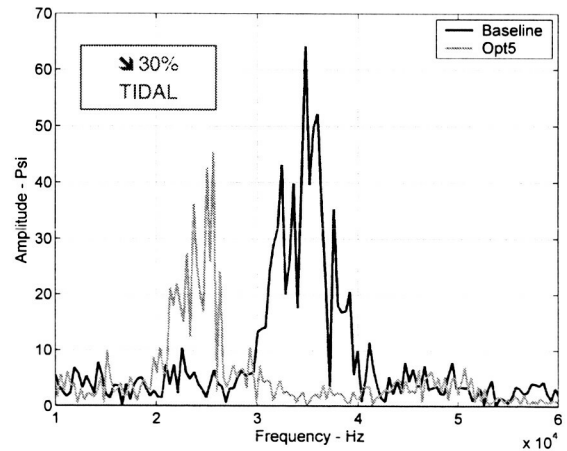
Figure 17. Comparison of TE pressure fluctuation due to vortex shedding obtained from Tidal 3-D CFD. Amplitude is reduced by 30% while frequency is reduced by 10 kHz.
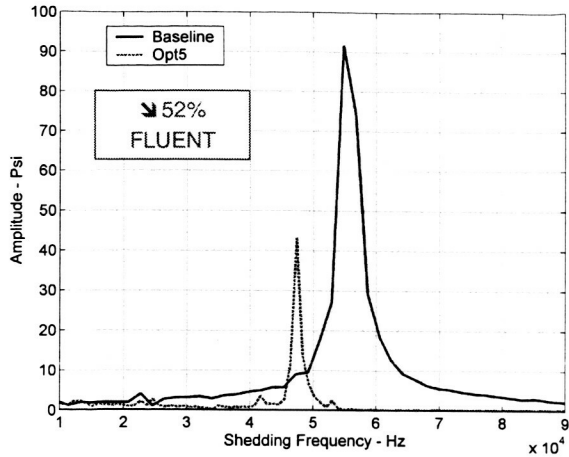
Figure 18. Comparison of TE pressure fluctuation due to vortex shedding obtained from FLUENT 2-D CFD. Amplitude is reduced by 50% while frequency is reduced by 9 kHz.
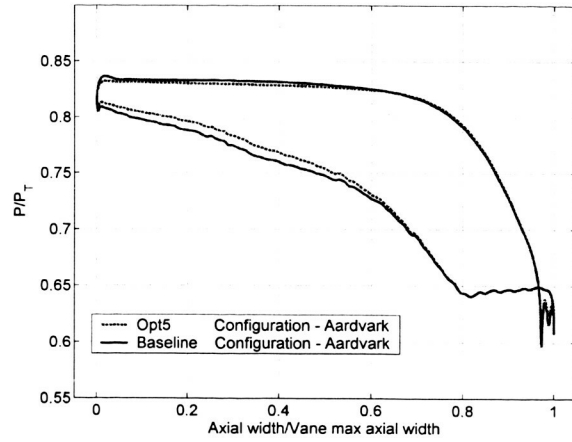
Figure 20. 2nd stage stator vane time averaged pressure load comparison between baseline and O5 nozzle configuration. Shown is Aardvark 2-D CFD solution.
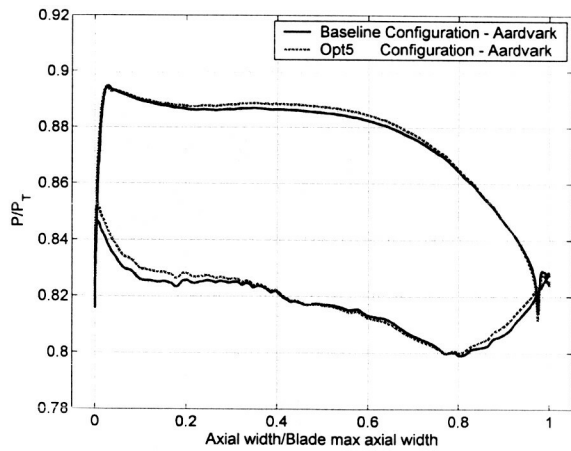

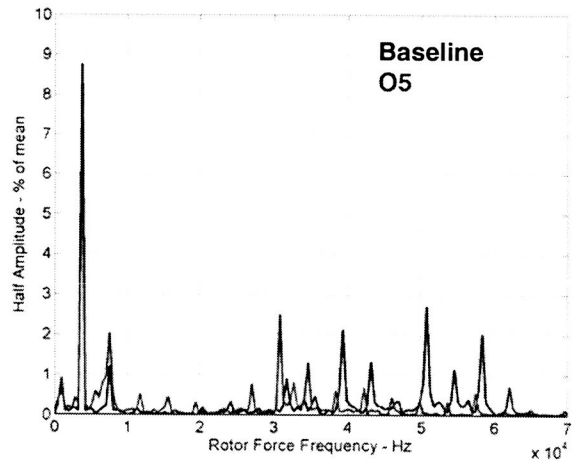Figure 19. 1st stage rotor blade time averaged pressure load comparison between baseline and O5 nozzle configuration. Shown is Aardvark 2-D CFD solution.

Figure 21. 1st stage rotor blade time unsteady tangential force FFT analysis, Aardvark 2-D CFD solution .
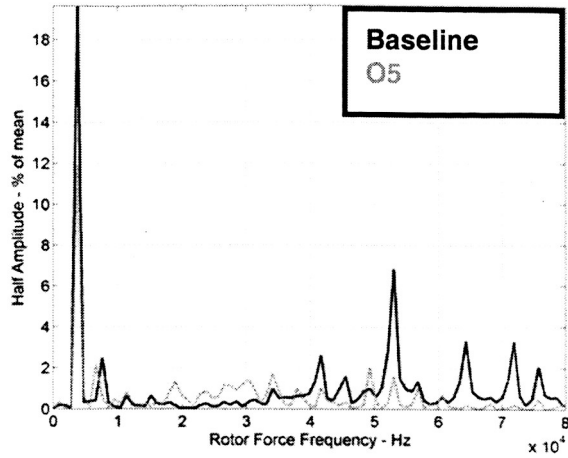
Figure 22. 1st stage rotor blade time unsteady tangential force FFT analysis, Wildcat 2-D CFD solution .
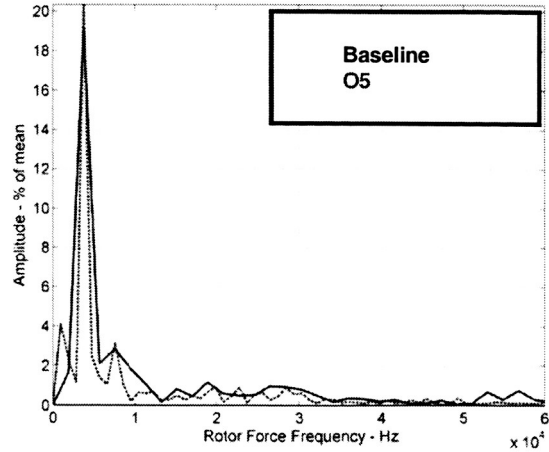

Figure 24. 1st stage rotor blade time unsteady tangential force FFT analysis, FLUENT 2-D CFD solution .
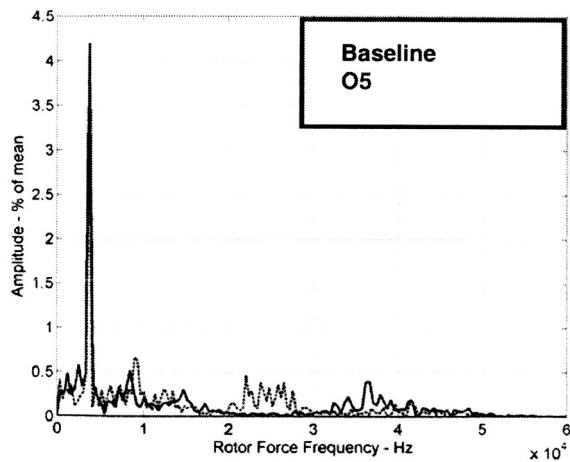

Figure 23. 1st stage rotor blade time unsteady tangential force FFT analysis, Tidal 3-D CFD solution .
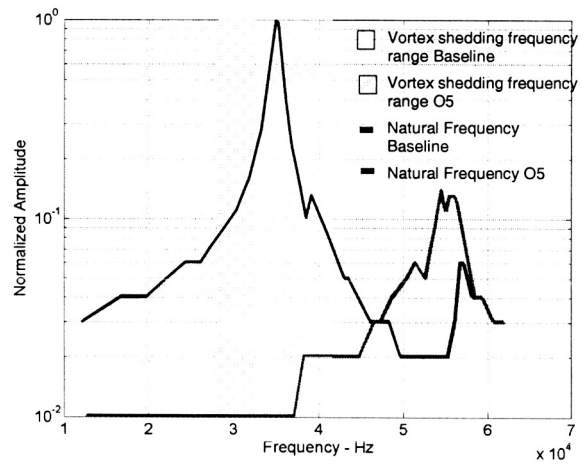

Figure 25. Vane natural frequencies associated with the trailing edge flap mode, baseline versus O5 comparison. The values are corrected for LOX mass flow effect by 30%. Shown are also the ranges for vortex shedding frequencies, based on Aardvark 2-D CFD with 20% correction based on calibration calculations using cylinders.
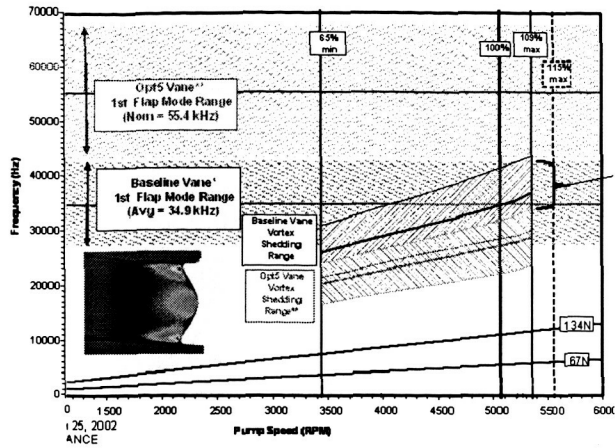
Figure 26. Campbell diagram for the nozzle vane. Shown are the ranges for vane natural frequencies associated with the TE flap mode and the shedding frequencies range and variation with engine RPL. While baseline geometry shows possible interference at all RPL's, redesigned O5 still has a margin of 27% (marked with accolade) at 109% RPL.
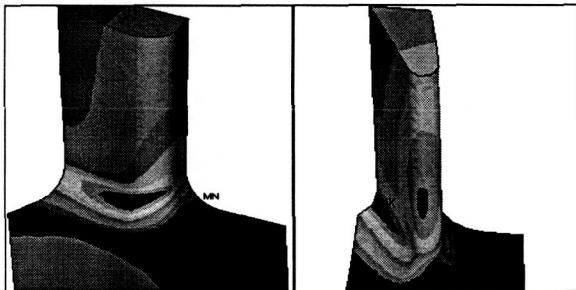
Leading Edge   Trailing Edge

Figure 27. Maximum stress locations on the first stage rotor blade occur at LE and TE. Loading for the calculations has been provided from Aardvark 2-D CFD calculations. The larger stress from the two local maxima occurs at the LE where in O5 the factor of safety for the rotor blade increases from 4.91 (baseline) to 6.31.

TABLE 1

load step	MEMBRANE (ksi)				BENDING (ksi)				TOTAL STRESS (ksi)		
	BL	OP 5	% CHANGE		BL	OP 5	% CHANGE		BL	OP 5	% CHANGE
MAX. STRESS DUE TO RADIAL & AXIAL BC	7.58	5.79	-31%		3.44	3.50	2%		11.02	9.29	-19%
MAX. STRESS DUE TO STATOR BLOWOFF LOAD	4.05	0.83	-390%		1.85	0.06	-2777%		5.89	0.89	-562%
MAX. STRESS DUE TO VANE PRESSURE ONLY	11.52	7.84	-47%		6.68	1.28	-423%		18.20	9.11	-100%
MAX OPERATION SILVER SEAL BOTTOM AT OD	29.50	22.22	-33%		22.42	15.78	-42%		51.92	38.00	-37%